

Acta Crystallographica Section B

**Structural Science,
Crystal Engineering
and Materials**

ISSN 2052-5206

Structure of Pb-rich chabournéite from Jas Roux, France

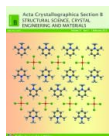
Cristian Biagioni, Yves Moëlo, Georges Favreau, Vincent Bourgoïn and Jean-Claude Boulliard

Acta Cryst. (2015). **B71**, 81–88

Copyright © International Union of Crystallography

Author(s) of this paper may load this reprint on their own web site or institutional repository provided that this cover page is retained. Republication of this article or its storage in electronic databases other than as specified above is not permitted without prior permission in writing from the IUCr.

For further information see <http://journals.iucr.org/services/authorrights.html>



Acta Crystallographica Section B: Structural Science, Crystal Engineering and Materials publishes scientific articles related to the structural science of compounds and materials in the widest sense. Knowledge of the arrangements of atoms, including their temporal variations and dependencies on temperature and pressure, is often the key to understanding physical and chemical phenomena and is crucial for the design of new materials and supramolecular devices. *Acta Crystallographica B* is the forum for the publication of such contributions. Scientific developments based on experimental studies as well as those based on theoretical approaches, including crystal-structure prediction, structure–property relations and the use of databases of crystal structures, are published.

Crystallography Journals Online is available from journals.iucr.org

Structure of Pb-rich chabournéite from Jas Roux,
FranceCristian Biagioni,^{a*} Yves Moëlo,^b
Georges Favreau,^c Vincent
Bourgoin^d and Jean-Claude
Boulliard^e^aDipartimento di Scienze della Terra, Università
di Pisa, Via Santa Maria 53, I-56126 Pisa, Italy,^bInstitut des Matériaux Jean Rouxel, UMR 6502,
CNRS, Université de Nantes, 2 rue de la

Houssinière, 44 322 Nantes CEDEX 3, France,

^c421 avenue Jean Monnet, 13090 Aix-en-Provence,
France, ^d24 rue Mozart, 93160 Noisy-le-Grand, France, and ^eCollection des minéraux de
l'UPMC-Sorbonne Universités, case courrier 73,
4 place Jussieu, 75252 Paris CEDEX 5, France

Correspondence e-mail: biagioni@dst.unipi.it

Received 15 September 2014

Accepted 26 December 2014

The crystal structure of a specimen of 'Pb-rich' chabournéite from Jas Roux, Hautes-Alpes, France, with the chemical formula obtained by electron microprobe analysis of $\text{Ag}_{0.04} (1) \text{Tl}_{2.15} (2) \text{Pb}_{0.64} (1) \text{Sb}_{5.12} (1) \text{As}_{5.05} (1) \text{S}_{17.32} (5)$, has been solved by X-ray single-crystal diffraction on the basis of 36 550 observed reflections (with $F_o > 4\sigma F_o$) with a final $R_1 = 0.074$. Pb-rich chabournéite is triclinic $P1$, with unit-cell parameters $a = 8.5197 (4)$, $b = 42.461 (2)$, $c = 16.293 (8) \text{ \AA}$, $\alpha = 83.351 (2)^\circ$, $\beta = 90.958 (2)^\circ$, $\gamma = 84.275 (2)^\circ$, $V = 5823 (3) \text{ \AA}^3$. Its structural formula is close to $[\text{Tl}_2(\text{Pb}_{0.8}\text{Tl}_{0.1}\text{Sb}_{1.1})](\text{Sb}_{4.1}\text{As}_{4.9})\text{S}_{17}$, with $Z = 8$. Its crystal structure is formed by the alternation of two pairs of slabs along the **b** axis, deriving from the SnS and PbS archetypes, respectively. 104 independent cation sites and 136 S sites occur in the unit cell. Slab interfaces show the alternation, along **c**, of Tl sites, ninefold coordinated, with Pb, Sb or mixed/split (Pb,Sb) and (Pb,Tl) sites. Within the slabs, 72 independent M^{3+} sites ($M^{3+} = \text{As}, \text{Sb}$) occur. Considering M^{3+} —S bond distances shorter than 2.70 Å, MS_3 triangular pyramidal groups are condensed according to various $M_m\text{S}_n$ chain fragments ('polymers'). The solution of the crystal structure of chabournéite allows its comparison with the closely related homeotypes protochabournéite and dalnegroite.

1. Introduction

Thallium concentration in the Earth's continental crust is 0.52 p.p.m. (Wedepohl, 1995). Notwithstanding its very low concentration, thallium is relatively more abundant than other well known elements, such as Ag (average crustal concentration 0.07 p.p.m.), Sb (0.2 p.p.m.) and Hg (0.04 p.p.m.). On the contrary, whereas Ag, Sb and Hg minerals are well known (170, 250 and 93 known mineral species, respectively), only 57 Tl minerals have been described so far; among them, 37 are represented by sulfosalts. This apparent discrepancy is related to the geochemical behavior of Tl that follows the fate of K^+ and Rb^+ , being hosted in silicates (*e.g.* mica, feldspar). Tl can be highly enriched in hydrothermal ore deposits in some circumstances, as it occurs in some classical localities such as Lengenbach, Binn Valley, Switzerland (Hofmann & Knill, 1996), Allchar, Macedonia (Volkov *et al.*, 2006), Jas Roux, Hautes-Alpes, France (Johan & Mantienne, 2000), and the Carlin type deposits, Nevada, USA (Cline *et al.*, 2005). Recently, new occurrences of thallium minerals have been reported from China (*e.g.* Lanmuchang, Guizhou Province – Xiao, 2001; Xiangquan, Anhui Province – Zhou *et al.*, 2005) and Italy (Vulcano island, Sicily – Campostrini *et al.*, 2011; Monte Arsiccio mine, Tuscany – Biagioni *et al.*, 2013).

The recent descriptions of the two new thallium sulfosalts dalnegroite (Nestola *et al.*, 2009) and protochabournéite

Table 1

Experimental details.

Crystal data	
X-ray formula	$\text{Ti}_{2.11}\text{Pb}_{0.76}(\text{Sb}_{5.19}\text{As}_{4.94})_{\Sigma 10.13}\text{S}_{17}$
M_r	17 088.93
Crystal system, space group	Triclinic, $P1$
Temperature (K)	293
a, b, c (Å)	8.5197 (4), 42.461 (2), 16.293 (8)
α, β, γ (°)	83.351 (2), 90.958 (2), 84.275 (2)
V (Å ³)	5823 (3)
Z	1
Radiation type	Mo $K\alpha$
μ (mm ⁻¹)	27.56
Crystal size (mm)	0.33 × 0.20 × 0.08
Data collection	
Diffractometer	Bruker SMART Breeze
Absorption correction	Multi-scan <i>SADABS</i> (Sheldrick 1996)
T_{\min}, T_{\max}	0.002, 0.010
No. of measured, independent and observed [$I > 2\sigma(I)$] reflections	153 075, 80 060, 36 550
R_{int}	0.043
$R\sigma$	0.0862
$(\sin \theta/\lambda)_{\max}$ (Å ⁻¹)	0.840
Refinement	
$R[F^2 > 2\sigma(F^2)], wR(F^2), S$	0.074, 0.203, 1.07
No. of reflections	80 060
No. of parameters	2160
No. of restraints	3
$\Delta\rho_{\max}, \Delta\rho_{\min}$ (e Å ⁻³)	5.30, -6.03
Absolute structure	Refined as an inversion twin
Absolute structure parameter	0.478 (7)

Computer programs: *SHELX97* (Sheldrick, 2008).

(Orlandi *et al.*, 2013) from the Lengenbach quarry and the Monte Arsiccio mine, respectively, allowed the definition of the chabournéite homeotypic series. Unfortunately, as pointed out by Orlandi *et al.* (2013), the exact definition of chabournéite is unclear, probably being a solid solution between a 'Pb-rich' chabournéite, $[\text{Ti}_2\text{PbSb}]_{\Sigma 4}(\text{Sb}_5\text{As}_4)\text{S}_{17}$, and a 'Pb-free' chabournéite, $[\text{Ti}_2(\text{Ti}_{0.5}\text{Sb}_{0.5})\text{Sb}]_{\Sigma 4}(\text{Sb}_4\text{As}_5)\text{S}_{17}$. Mantiene (1974), in his preliminary description of chabournéite, reported chemical data close to the 'Pb-rich' composition, whereas the second, more accurate definition given by Johan *et al.* (1981) corresponded to the 'Pb-free' pole. In addition, the crystal structure of chabournéite (actually the 'Pb-rich' chabournéite) reported by Nagl (1979) was based on the sub-cell ('old structure' hereafter, *i.e.* Och), so requiring a more accurate refinement in order to perform a careful comparison with the crystal structures of the two related species dalnegroite and protochabournéite.

Recently, a new field and laboratory study of the Jas Roux thallium mineralization (Favreau *et al.*, 2011) allowed the collection of further material. In the studied specimen, collected in the C1 area, chabournéite occurs as a small metallic black compact mass, associated with abundant wakabayashilite and realgar. Using this sample we were able to solve and refine the true crystal structure of chabournéite ('new structure' hereafter, *i.e.* Nch), achieving a better understanding of its crystal chemistry and its relationships with other members of the chabournéite homeotypic series.

2. Experimental

For the X-ray single-crystal study, the intensity data were collected using a Bruker SMART Breeze diffractometer equipped with an air-cooled CCD detector, with Mo $K\alpha$ radiation. The detector-to-crystal distance was 50 mm. 3755 frames were collected using ω and ϕ scan modes, in 0.5° slices, with an exposure time of 25 s per frame. The data were corrected for the Lorentz and polarization factors, and absorption using the software package *APEX2* (Bruker, 2004). Unit-cell parameters are $a = 8.5197$ (4), $b = 42.461$ (2), $c = 16.293$ (8) Å, $\alpha = 83.351$ (2), $\beta = 90.958$ (2), $\gamma = 84.275$ (2)°, $V = 5823$ (3) Å³. No systematic absences were observed, implying a choice of space groups $P1$ or $P\bar{1}$. The statistical tests on the distribution of $|E|$ values ($|E^2 - 1| = 0.983$) suggested the centrosymmetry of the structure that was initially solved through direct methods using *SHELXS97* (Sheldrick, 2008). However, it was not possible to obtain a reliable structural model. Consequently, a new crystal structure solution was tried in the noncentrosymmetric $P1$ space group. After having located the heavier atoms, the structure was refined using *SHELXL97* (Sheldrick, 2008) and completed through several successive difference-Fourier maps. Scattering curves for neutral atoms were taken from *International Tables for Crystallography* (Wilson, 1992). Crystal data and details of the intensity data collection and refinement are reported in Table 1. After several cycles of isotropic refinement, R_1 converged to 0.124. Successive cycles of refinement gave $R_1 = 0.080$, with an anisotropic model for all the atoms, with the exception of some S atoms that have anisotropic displacement parameters were negatively defined. Mixed (Pb,Sb), (Pb,Tl) and (As,Sb) sites were discriminated on the basis of their Z total; their site occupancies were then adjusted on the basis of bond-valence calculations, whereas the site occupancies of split sites were refined only with their Z total. Finally, the refinement converged to $R_1 = 0.074$ for 36 550 reflections with $F_o > 4\sigma(F_o)$ and 0.154 for all 80 060 independent reflections. The unit-cell content is shown in Fig. 1. A figure with atom labels (Fig. S1), as well as the CIF of chabournéite, are available as supporting information.

The crystal used for the intensity data collection was then embedded in epoxy and used for chemical analysis. Electron-microprobe analyses were carried out with a CAMECA SX100 apparatus at 20 kV and 20 nA, with a 1 µm beam

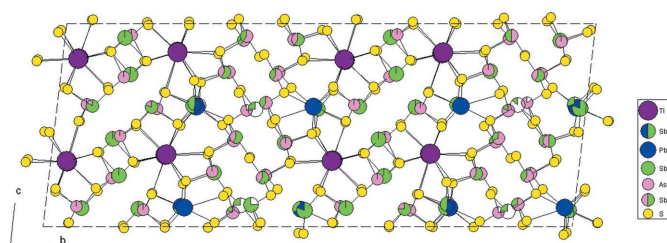


Figure 1
Projection along **a** of the unit cell of Pb-rich chabournéite. Atoms in order of decreasing size: Tl (violet), Pb (blue), Sb (green), As (pink) and S (yellow).

Table 2

Average bond distances (Å) and bond valence sums (v.u.) for pure Tl sites in chabournéite. Bond valence sums are calculated according to the parameters given by Brese & O’Keeffe (1991); the values within brackets have been calculated using $R_{\text{Tl,S}} = 2.55$ Å.

Site	$\langle \text{Tl}-\text{S} \rangle$	BVS	Site	$\langle \text{Tl}-\text{S} \rangle$	BVS	Site	$\langle \text{Tl}-\text{S} \rangle$	BVS	Site	$\langle \text{Tl}-\text{S} \rangle$	BVS
Tl1	3.364	1.29 (1.04)	Tl2	3.380	1.22 (0.98)	Tl3	3.390	1.22 (0.98)	Tl4	3.341	1.43 (1.15)
Tl5	3.410	1.17 (0.95)	Tl6	3.363	1.35 (1.09)	Tl7	3.377	1.24 (1.00)	Tl8	3.382	1.21 (0.97)
Tl9	3.388	1.23 (0.99)	Tl10	3.343	1.43 (1.15)	Tl11	3.361	1.30 (1.04)	Tl12	3.379	1.22 (0.98)
Tl13	3.358	1.31 (1.05)	Tl14	3.364	1.26 (1.02)	Tl15	3.389	1.24 (1.00)	Tl16	3.339	1.43 (1.15)

diameter. Standards (element, emission line, counting time) are: galena (Pb $M\alpha$, 60 s), stibnite (Sb $L\alpha$, 60 s), AsGa (As $L\alpha$, 30 s), pyrite (S $K\alpha$, 60 s), Ag (Ag $L\alpha$, 30 s) and lorándite (Tl $M\alpha$, 20 s). Analytical results are (in wt% – average of 4 spot analyses): Ag 0.22 (3), Tl 20.29 (5), Pb 6.13 (10), Sb 28.81 (33), As 17.48 (23), S 25.66 (27), total 98.58 (91). On the basis of $\Sigma M = 13$ atoms per formula unit (*apfu*), the empirical formula for the studied crystal is $\text{Ag}_{0.04}(\text{Tl}_{2.15})\text{Pb}_{0.64}(\text{Sb}_{5.12})\text{As}_{5.05}\text{S}_{17.32}$. The valence equilibrium value, E_v (%), defined as $[\Sigma(\text{val}+) - \Sigma(\text{val}-)] \times 100/\Sigma(\text{val}-)$, is -1.9 (3). After the subtraction of Ag, in agreement with the heterovalent substitution $\text{Ag}^+ + \text{Sb}^{3+} = 2\text{Pb}^{2+}$, the formula can be written as $\text{Tl}_{2.15}\text{Pb}_{0.72}\text{Sb}_{5.08}\text{As}_{5.05}\text{S}_{17.32}$. On the basis of the general structural formula of the members of the chabournéite series, $[\text{Tl}_2 - x\text{Pb}_1 + 2x\text{Sb}_1 - x]_{\Sigma 4}(\text{Sb}_9 - y\text{As}_y)\text{S}_{17}$, proposed on the basis of the primitive cell (Orlandi *et al.*, 2013), one obtains $x \simeq -0.15$, $y = 5.05$. With the atom ratios Sb/(Sb + As) and Pb/(Pb + 2Tl) equal to 0.501 and 0.143, respectively, it corresponds to a ‘Pb-rich’ chabournéite (see Fig. 9 of Orlandi *et al.*, 2013).

3. Crystal structure description

3.1. General organization of chabournéite

Fig. 2 is an enlarged projection along **a** of the crystal structure of chabournéite. It agrees with the general features of Och given by Nagl (1979). Actually, whereas in the crystal structure reported by this author all the cation positions correspond to pure Tl, Pb, Sb or As sites, the real structure Nch of chabournéite also presents mixed (Pb/Tl), (Pb/Sb) and (As/Sb) sites.

Although chabournéite is not a layered compound, its crystal structure can be described as formed by the alternation of four slabs (Fig. 2) of two kinds (Makovicky, 1985). Two of them correspond to the ‘thin slab’ *t* reported by Orlandi *et al.* (2013) for protochabournéite, and they will be indicated as **t**₁ and **t**₂. They derive from the SnS archetype and are closely related to sartorite (Berlepsch *et al.*, 2003) and parapierrrotite (Engel, 1980). The other two slabs correspond to the ‘thick slab’ *T* of protochabournéite and are related to the PbS archetype; they will be indicated as **T**₁ and **T**₂. The inner part of these *T* slabs can be described as ‘rod-layers’, which belong to Type 2 of Makovicky (1993).

3.2. Cation coordination and site occupancies

The new crystal structure of chabournéite (Nch) shows 104 independent cation sites and 136 S positions.

Sixteen pure Tl sites occur (Table 2), having a triangular prismatic coordination with three capping ligands. Average $\langle \text{Tl}-\text{S} \rangle$ bond distances range between 3.339 (8) (for Tl16) and 3.410 (8) Å (for Tl5), in very good agreement with the results given by Nagl (1979); single bond distances range from 3.166 (8) (Tl16–S105) to 3.667 (7) Å (Tl10–S69). Tl sites occur in the mono-atomic zigzag surfaces separating the *t* and *T* slabs. Columns of Tl-centered polyhedra, running along [100], alternate, along [001], with columns of polyhedra having different occupancies, *i.e.* pure Sb, mixed (Sb,Pb), (Pb,Sb), (Pb,Tl) and split (Pb,Sb), (Sb,Pb) and (Sb,Sb) sites. Bond valence sums (BVS), calculated according to the parameters given by Brese & O’Keeffe (1991), indicate a constant oversaturation of pure Tl sites (Table 2), with values ranging between 1.18 and 1.43 v.u. (valence units), with an average value of 1.28 v.u. This oversaturation, which could be interpreted as due to a mixed (Tl,Pb) site occupancy, is due to an artefact of the BVS calculation, as follows.

In the paper describing protochabournéite, Orlandi *et al.* (2013) re-examined the crystal structure given by Nagl (1979) for chabournéite (Och) and proposed a new cation distribution based on BVS calculation. The proposed cation distri-

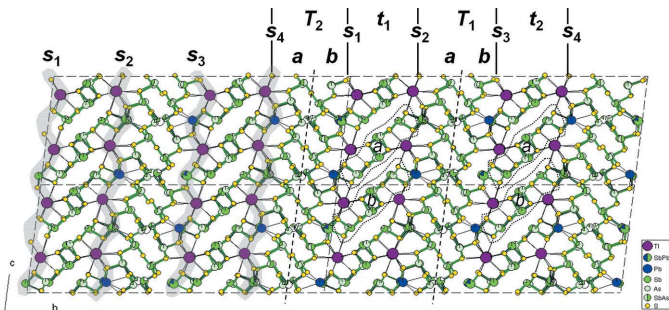


Figure 2 Enlarged projection along **a** of the crystal structure of Pb-rich chabournéite, showing its layered organization (thin *t* and thick *T* slabs). The tie-lines within the *T* slabs represent surfaces of weak bonding separating two sub-slabs. The dotted lines within the *t* slabs indicate the sartorite-type ribbon. **s**₁ to **s**₄ (shaded in grey): mono-atomic zigzag interfaces M_8S_8 with heavy atoms (Tl, Pb and Sb) connecting the *t* and *T* slabs.

Table 3

Average bond distance (Å), and bond valence sums (v.u.) for Pb and Sb sites occurring in the zigzag monoatomic surfaces separating the *t* and *T* slabs in chabournéite.

Bond valence sums are calculated according to the parameters given by Brese & O'Keeffe (1991). Expected values, calculated according to the site occupancies, are reported within brackets.

Site	$\langle M-S \rangle$	BVS	Site	$\langle M-S \rangle$	BVS	Site	$\langle M-S \rangle$	BVS	Site	$\langle M-S \rangle$	BVS
Sb1	2.921	2.75 (2.80)	Pb2a	3.008	2.02 (1.72)	Sb2b	2.949	0.37 (0.42)	Pb3	3.176	1.75 (1.75)
Sb4	2.959	2.77 (3.00)	Sb5a	2.940	1.68 (1.77)	Sb5b	3.020	1.07 (1.23)	Pb6a	3.027	0.87 (0.82)
Sb6b	3.090	1.51 (1.77)	Pb7	3.195	1.80 (1.80)	Sb8	2.979	2.86 (2.70)	Pb9	3.171	1.79 (1.80)
Sb10	2.954	2.81 (3.00)	Sb11	3.026	2.83 (2.80)	Pb12	3.092	2.26 (2.30)	Pb13	3.180	1.82 (1.80)
Sb14	2.958	2.74 (3.00)	Sb15a	2.929	1.44 (1.59)	Sb15b	3.061	1.34 (1.41)	Pb16a	3.003	0.90 (0.82)
Sb16b	3.106	1.60 (1.77)	—	—	—	—	—	—	—	—	—

bution for Och was in close agreement with the chemical data given by Nagl (1979) considering the $As/(As + Sb)_{at}$ ratio, whereas it showed a $Pb/(Pb + Tl)_{at}$ ratio significantly higher than that reported in the original paper (Nagl, 1979). Such a high ratio is probably the result of using an inappropriate value of R_{ij} for the Tl—S bond; following Biagioni *et al.* (2014), better agreement between observed and expected BVS for Tl sites can be achieved using a value of $R_{Tl,S} = 2.55$ Å (values within brackets of Table 2). In this way, only three Tl sites in the 8 Å structure of chabournéite (Nch), namely Tl4, Tl10 and Tl16, are slightly oversaturated. In agreement with these observations, it is interesting to note that Orlandi *et al.* (2013) fixed the site occupancies of Tl and Pb sites in protochabournéite on the basis of the BVS, obtaining a $Pb/(Pb + Tl)_{at}$ ratio slightly higher than those observed in the chemical analyses. On the contrary, by using the $R_{Tl,S}$ value suggested by Biagioni *et al.* (2014), good agreement between the $Pb/(Pb + Tl)_{at}$ ratio obtained during the crystal structure study and the chemical analysis of protochabournéite can be achieved too.

Alternating with Tl sites along [001] in the mono-atomic zigzag surfaces separating the *t* and *T* slabs, columns of Pb and Sb sites running along [100] occur (Table 3). Two different kinds of Pb—Sb columns alternate along [001]; one is formed by the alternation of mixed (Pb,Tl) sites with pure Sb or mixed (Sb,Pb) sites, whereas the other is composed by mixed (Sb,Pb) or (Pb,Sb) alternating with split (Pb,Sb), (Sb,Pb) and (Sb,Sb) sites.

Four mixed (Pb,Tl) sites occur, namely Pb3, Pb7, Pb9 and Pb13. They have an eightfold coordination, with average bond distances ranging from 3.171 Å for Pb9 to 3.195 Å for Pb7. Their BVS values range between 1.75 (Pb3 site) and 1.82 v.u.; on this basis, their s.o.f. (site occupancy factor) was fixed.

Three pure Sb sites occur, namely Sb4, Sb10 and Sb14; they alternate along [100] with mixed (Pb,Tl) sites. Their BVS ranges between 2.74 and 2.81 v.u.

Three mixed (Sb,Pb) sites, *i.e.* Sb1, Sb8 and Sb11, and one mixed (Pb,Sb) site, *i.e.* Pb12, are present in the crystal structure of this Pb-rich chabournéite. On the basis of their BVSs, their s.o.f. was fixed to $(Sb_{0.80}Pb_{0.20})$. The mixed (Pb,Sb) site,

Pb12, has a site occupancy $(Pb_{0.70}Sb_{0.30})$ adjusted on the basis of its BVS (2.26 v.u.).

Finally, five split sites, (Sb,Sb) or mixed (Pb,Sb), occur. Sb5 and Sb15 are split into two sub-positions (Sb5a, Sb5b) and (Sb15a, Sb15b), respectively. Sb5a and Sb15a show the typical triangular pyramidal coordination, with three Sb—S distances shorter than 2.70 Å, with average bond distances of 2.508 and 2.530 Å for Sb5a and Sb15a, respectively. Three split (Pb,Sb) or (Sb,Pb) sites, namely (Pb2a, Sb2b), (Pb6a, Sb6b) and (Pb16a, Sb16b), complete the set of sites forming the mono-atomic zigzag surfaces separating the *t* and *T* slabs.

There are 72 independent M^{3+} sites ($M^{3+} = As, Sb$) which form the *T* and *t* slabs (Table 4). Each *t* slab is composed of 16 M^{3+} sites, whereas 20 M^{3+} sites occur in each *T* slab. Among the M^{3+} sites, 18 are pure Sb sites, 18 pure As sites and 36 mixed (As,Sb) or (Sb,As) sites. Among the latter, 23 are As-dominant sites, *i.e.* (As,Sb). Table 4 gives the average bond distances for these M^{3+} sites and the corresponding BVS values. As stated above, the site occupancies of unsplit M^{3+} sites have been adjusted on the basis of BVS calculations; on the contrary, the site occupancy of the split (Sb/As) positions were refined only on the basis of their *Z* total. Their BVS values usually indicate a slight undersaturation, with values ranging from 2.55 v.u. for the pair Sb87a/As87b to 2.68 v.u. for the pair Sb42a/Sb42b. On the other hand, the BVS of the pair Sb51a/Sb51b shows an important oversaturation (3.72 v.u.), thus indicating that Sb is partially replaced by As, the latter probably being preferentially hosted at the smaller Sb51a sub-site.

3.3. Polymerization of $M^{3+}S_3$ triangular pyramidal polyhedra

Within the slabs, the examination of the sub-organization of M^{3+} sites, taking into account only the shortest M^{3+} —S bond distances (shorter than 2.70 Å, in agreement with the approach used by Moëlo *et al.*, 2012), allows the description of their organization into finite $M^{3+}_mS_n$ chain fragments (pseudo-polymers or 'polymers' hereafter).

In the *t* layers, four sartorite-type ribbons can be selected (namely *t*_{1a}, *t*_{1b}, *t*_{2a} and *t*_{2b} – Fig. 2). As reported in other

Table 4Average bond distances (Å) and bond valence sums (v.u.) for M^{3+} sites occurring in the \mathbf{t} and \mathbf{T} slabs in chabournéite.Bond valence sums are calculated according to the parameters given by Brese & O'Keeffe (1991). Average $\langle M^{3+}-S \rangle$ distances are calculated for distances shorter than 2.70 Å. Bond-valence sums are calculated according to the site occupancy.

Site	$\langle M-S \rangle$	BVS	Site	$\langle M-S \rangle$	BVS	Site	$\langle M-S \rangle$	BVS	Site	$\langle M-S \rangle$	BVS
Sb17	2.502	3.03	As18	2.290	2.97	As19	2.289	2.96	Sb20	2.493	3.05
Sb21	2.472	3.14	As22	2.269	3.06	Sb23	2.504	2.86	As24	2.286	2.92
As25	2.290	3.15	Sb26	2.490	3.08	Sb27	2.495	3.06	As28	2.285	2.97
As29	2.260	3.15	Sb30	2.514	3.09	As31	2.293	3.06	Sb32	2.514	3.05
As33	2.392	2.98	As34	2.374	3.17	Sb35	2.435	3.06	As36	2.416	3.08
Sb37	2.446	2.92	As38	2.398	3.06	As39	2.402	3.06	As40	2.414	3.06
As41	2.352	3.13	Sb42a	2.577	0.70	As42b	2.326	1.98	Sb43	2.446	2.95
As44	2.375	3.04	As45	2.278	3.10	Sb46	2.554	2.89	As47	2.287	3.00
Sb48	2.569	2.81	Sb49	2.446	3.05	As50	2.374	2.87	Sb51a	2.382	2.87
Sb51b	2.460	0.85	As52	2.341	2.87	As53	2.285	2.96	Sb54	2.494	3.06
Sb55	2.492	3.12	As56	2.291	2.98	As57	2.277	3.01	Sb58	2.505	3.12
As59	2.279	3.00	Sb60	2.515	3.04	Sb61	2.487	3.15	As62	2.287	3.00
As63	2.292	2.93	Sb64	2.479	3.16	Sb65	2.488	2.93	As66	2.284	2.94
Sb67	2.487	2.89	As68	2.261	3.12	As69	2.421	3.00	As70	2.358	3.04
As71	2.281	3.07	Sb72	2.549	2.94	As73	2.262	3.21	Sb74	2.570	2.81
Sb75	2.454	3.02	As76	2.361	2.96	As77a	2.343	2.16	Sb77b	2.533	0.47
As78	2.335	2.93	As79	2.377	2.92	As80	2.386	2.92	As81	2.419	3.01
As82	2.406	2.98	Sb83	2.438	3.02	As84	2.403	2.89	As85	2.434	2.94
As86	2.399	3.01	Sb87a	2.602	0.65	As87b	2.343	1.90	As88	2.321	3.22

phases characterized by the occurrence of sartorite-type layers, chabournéite presents a central 'polymer', here $[\text{Sb}_3\text{As}(\text{As},\text{Sb})(\text{Sb},\text{As})]_{\Sigma 6}\text{S}_{10}$, with two lateral AsS_3 or $(\text{As},\text{Sb})\text{S}_3$ groups (Fig. 3). Such a type of configuration, $(\text{AsS}_3)_2[\text{Sb}_3\text{As}(\text{As},\text{Sb})(\text{Sb},\text{As})]_{\Sigma 6}\text{S}_{10}$, agrees with that observed by Nagl (1979) for Och, $(\text{AsS}_3)_2[\text{Sb}_4\text{As}_2]_{\Sigma 6}\text{S}_{10}$. Minor replacements of Sb by As occur in the central 'polymers', whereas minor substitutions of As by Sb have been observed in the central 'polymers' and as well as at the isolated AsS_3 positions. The $\text{As}/(\text{As} + \text{Sb})_{\text{at}}$ ratios in the central 'polymers' of $\mathbf{t_1a}$, $\mathbf{t_1b}$, $\mathbf{t_2a}$ and $\mathbf{t_2b}$ sartorite-type ribbons are 0.35, 0.36, 0.33 and 0.375, respectively. The As to Sb substitution in the central 'polymers' takes place at one end of the chain. In protochabournéite, the equivalent configuration characterizing the \mathbf{t} slab is $[(\text{Sb},\text{As})\text{S}_3]_2[\text{Sb}_4(\text{Sb},\text{As})]_{\Sigma 6}\text{S}_{10}$. Such polymeric configuration has also been reported in boscardinite, with composition $[(\text{Sb}_{0.71}\text{As}_{0.29})\text{S}_3]_2[\text{Sb}_4(\text{As}_{0.745}\text{Sb}_{0.255})]_{\Sigma 6}\text{S}_{10}$ (Orlandi *et al.*, 2012).

It is likely that a similar polymeric arrangement of $M^{3+}\text{S}_3$ pyramidal polyhedra also occurs in dalnegroite (Bindi *et al.*, 2010), but Sb and As atoms do not show the typical triangular pyramidal coordination probably owing to the quality of the crystal studied which did not permit the S atoms to be localized accurately (for instance, there are numerous short Sb—S distances below 2.45 Å [the bond valence parameter for the pair (Sb, S)], down to 1.94 Å).

Within the \mathbf{T} layers, if one omits the central Sb positions with low s.o.f. (No. Sb/s.o.f.: 42a/0.25, 51b/0.26, 77b/0.15 and 87a/0.25), each \mathbf{T} slab is separated into two sub-slabs, $\mathbf{T_a}$ and $\mathbf{T_b}$ (Fig. 2), which show a single type of 'polymer' $(\text{Sb},\text{As})_5\text{S}_9$ (Fig. 4 for $\mathbf{T_1}$):

sub- $\mathbf{T_1a}$: $\text{Sb}(\text{Sb}_{0.60}\text{As}_{0.40})(\text{Sb}_{0.40}\text{As}_{0.60})_2(\text{Sb}_{0.20}\text{As}_{0.80})\text{S}_9$ and $(\text{Sb}_{0.60}\text{As}_{0.40})(\text{Sb}_{0.40}\text{As}_{0.60})(\text{Sb}_{0.25}\text{As}_{0.75})\text{As}_2\text{S}_9$;

sub- $\mathbf{T_1b}$: $\text{Sb}(\text{Sb}_{0.60}\text{As}_{0.40})(\text{Sb}_{0.50}\text{As}_{0.50})(\text{Sb}_{0.40}\text{As}_{0.60})_2\text{S}_9$ and $\text{Sb}(\text{Sb}_{0.60}\text{As}_{0.40})(\text{Sb}_{0.50}\text{As}_{0.50})(\text{Sb}_{0.20}\text{As}_{0.80})\text{As}_2\text{S}_9$;

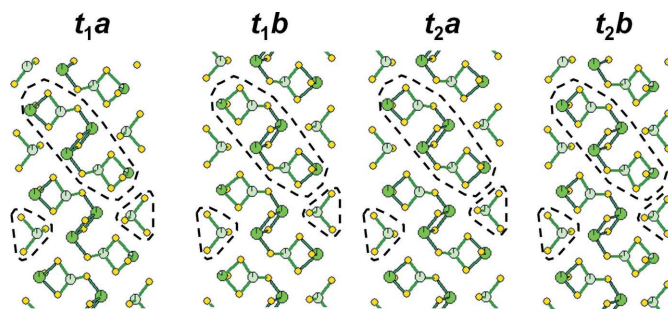
sub- $\mathbf{T_2a}$: $(\text{Sb}_{0.60}\text{As}_{0.40})(\text{Sb}_{0.50}\text{As}_{0.50})(\text{Sb}_{0.30}\text{As}_{0.70})_2(\text{Sb}_{0.20}\text{As}_{0.80})\text{S}_9$ and $(\text{Sb}_{0.50}\text{As}_{0.50})(\text{Sb}_{0.40}\text{As}_{0.60})(\text{Sb}_{0.20}\text{As}_{0.80})\text{As}_2\text{S}_9$;

sub- $\mathbf{T_2b}$: $\text{Sb}(\text{Sb}_{0.50}\text{As}_{0.50})(\text{Sb}_{0.40}\text{As}_{0.60})_2(\text{Sb}_{0.30}\text{As}_{0.70})\text{S}_9$ and $(\text{Sb}_{0.60}\text{As}_{0.40})(\text{Sb}_{0.40}\text{As}_{0.60})(\text{Sb}_{0.20}\text{As}_{0.80})\text{As}_2\text{S}_9$.

3.4. Role of 'bridging Sb' at the center of the \mathbf{T} layers

In $\mathbf{T_2b}$ sub-slab, for example, if As77a or As87b sites are substituted by Sb77b (s.o.f. 0.15) or Sb87a (s.o.f. 0.25), respectively, two $(\text{Sb},\text{As})_5\text{S}_9$ in-front 'polymers' are changed into one $(\text{Sb},\text{As})_3\text{S}_6$ and one $(\text{Sb},\text{As})_7\text{S}_{12}$ 'polymer' (Fig. 5). The biggest 'polymer' has the highest Sb/As ratio, with two Sb-pure sites, while inversely the smallest one, with the lowest Sb/As ratio, has one As-pure site.

The same approach in $\mathbf{T_1a}$, replacing As42b or Sb51a by Sb42a (s.o.f. 0.25) or Sb51b (s.o.f. 0.26), respectively, gives the same result.

**Figure 3**Polymeric organization of the M^{3+} atoms with S (short bonds) forming ribbons (tie-lines) in the \mathbf{t} slabs.

3.5. Role of 'bridging Sb' in the *t/T* polymeric connection

Sb atoms in the Sb-pure or mixed (Pb,Sb) sites of the zigzag surfaces, when present, connect 'polymers' of the two types of slabs. For instance, in the *t*₁/*T*₂ connection, Sb4 (s.o.f. 1) connects the As₂S₃ monomer and associated (Sb,As)₆S₁₀ 'polymer' of the *t*_{1a} ribbon with the (Sb,As)₅S₉ 'polymer' of the neighbouring *T*_{2b} 'polymer'. This last 'polymer' is connected along *c* to the next *t*_{1b} (Sb,As)₅S₉ 'polymer' via Sb1 (s.o.f. 0.80). On its other side, the (Sb,As)₆S₁₀ 'polymer' is connected to the *T*₁ layer via Sb5a (s.o.f. 0.59). In such a way, more complex 'polymers' are formed in a two-dimensional fashion; nevertheless, they are finite 'polymers', interrupted when Pb, and not Sb, is present in the mixed (Pb,Sb) site.

4. Crystal chemistry

4.1. Structural formula

The crystal-chemical formula of chabournéite, as obtained through the refinement of the crystal structure, is $\text{Ti}_{2.11}\text{Pb}_{0.76}(\text{Sb}_{5.19}\text{As}_{4.94})_{\Sigma 10.13}\text{S}_{17}$ (*Z* = 8), with an *Ev* value of +0.06. This formula can be compared with the formula

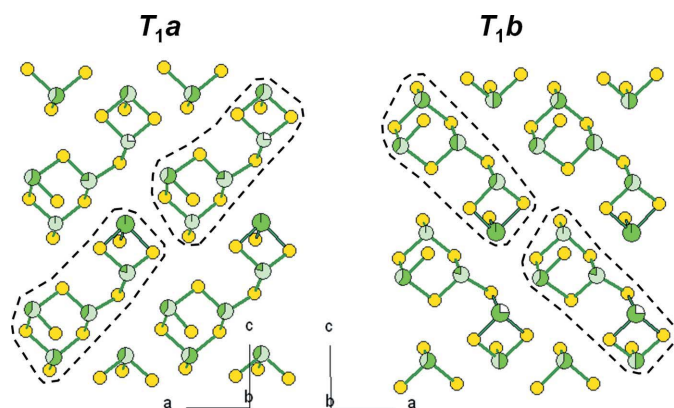


Figure 4
Polymeric organization of the M^{3+} atoms with S atoms (short bonds) in the *t*_{1a} and *T*_{1b} sub-slabs. Tie-lines surround in each sub-slab the two constitutive (Sb/As)₅S₉ polymers.

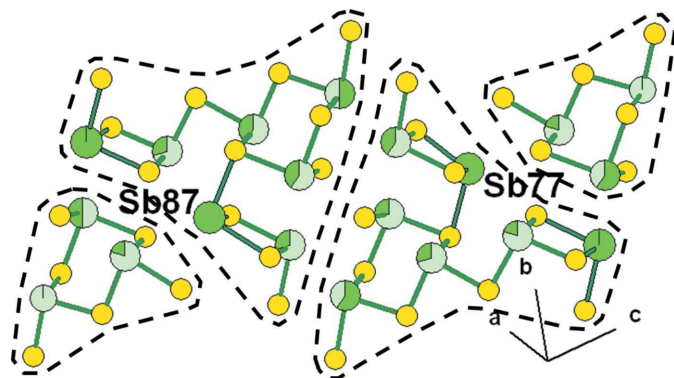


Figure 5
Sb connection within the *T*_{2a} sub-slab, forming (Sb/As)₃S₆ and (Sb/As)₇S₁₂ polymers.

$\text{Ti}_{2.15}\text{Pb}_{0.72}(\text{Sb}_{5.08}\text{As}_{5.05})_{\Sigma 10.13}\text{S}_{17.32}$, based on the chemical analysis of the studied crystal. Doubling this structural formula agrees with the general formula $\text{Ti}_{5-x}\text{Pb}_{2x}(\text{Sb,As})_{21-x}\text{S}_{34}$ proposed for chabournéite and protochabournéite, with $x \simeq 0.7$.

The four *t*₁, *t*₂, *T*₁ and *T*₂ slabs observed in the crystal structure of chabournéite (Fig. 2) present distinct chemical compositions. The mono-atomic zigzag surfaces *s*_n (Fig. 2) with heavy atoms common to these slabs have the compositions (in the +*b* direction):

$$\begin{aligned} s_1 &= \text{Ti}_4(\text{Pb}_{0.75}\text{Ti}_{0.25})(\text{Pb}_{0.86}\text{Sb}_{0.14})\text{Sb}(\text{Sb}_{0.80}\text{Pb}_{0.20})\text{S}_8 \quad \text{or} \\ &\text{Ti}_{4.25}\text{Pb}_{1.81}\text{Sb}_{1.94}\text{S}_8; \\ s_2 &= \text{Ti}_4(\text{Pb}_{0.80}\text{Ti}_{0.20})(\text{Sb}_{0.59}\text{Pb}_{0.41})\text{Sb}(\text{Sb}_{0.80}\text{Pb}_{0.20})\text{S}_8 \quad \text{or} \\ &\text{Ti}_{4.20}\text{Pb}_{1.41}\text{Sb}_{2.39}\text{S}_8; \\ s_3 &= \text{Ti}_4(\text{Pb}_{0.80}\text{Ti}_{0.20})(\text{Pb}_{0.70}\text{Sb}_{0.30})\text{Sb}(\text{Sb}_{0.80}\text{Pb}_{0.20})\text{S}_8 \quad \text{or} \\ &\text{Ti}_{4.20}\text{Pb}_{1.70}\text{Sb}_{2.10}\text{S}_8; \\ s_4 &= \text{Ti}_4(\text{Pb}_{0.80}\text{Ti}_{0.20})(\text{Sb}_{0.59}\text{Pb}_{0.41})\text{Sb}_2\text{S}_8 \quad \text{or} \\ &\text{Ti}_{4.20}\text{Pb}_{1.21}\text{Sb}_{2.59}\text{S}_8. \end{aligned}$$

The composition of the *t*₁ slab is obtained by adding half of the atoms of the surfaces *s*₁ and *s*₂ to the atoms between the zigzag surfaces:

$$\text{Ti}_{4.225}\text{Pb}_{1.61}\text{Sb}_{2.165}\text{S}_8 + (\text{As}_{8.15}\text{Sb}_{7.85})\text{S}_{24} = [\text{Ti}_{4.225}\text{Pb}_{1.61}\text{Sb}_{2.165}](\text{As}_{8.15}\text{Sb}_{7.85})\text{S}_{32}.$$

Analogously, slab *T*₁ has a composition which is obtained by adding half of the atoms of the surfaces *s*₂ and *s*₃ to the atoms between the surfaces:

$$\text{Ti}_{4.20}\text{Pb}_{1.555}\text{Sb}_{2.245}\text{S}_8 + (\text{As}_{10.70}\text{Sb}_{9.30})\text{S}_{28} = [\text{Ti}_{4.20}\text{Pb}_{1.555}\text{Sb}_{2.245}](\text{As}_{10.70}\text{Sb}_{9.30})\text{S}_{36}.$$

Similarly, slab *t*₂ has composition:

$$\text{Ti}_{4.20}\text{Pb}_{1.455}\text{Sb}_{2.345}\text{S}_8 + (\text{As}_{8.25}\text{Sb}_{7.75})\text{S}_{24} = [\text{Ti}_{4.20}\text{Pb}_{1.455}\text{Sb}_{2.345}](\text{As}_{8.25}\text{Sb}_{7.75})\text{S}_{32};$$

whereas the composition of the slab *T*₂ is:

$$\text{Ti}_{4.225}\text{Pb}_{1.51}\text{Sb}_{2.265}\text{S}_8 + (\text{As}_{12.40}\text{Sb}_{7.60})\text{S}_{28} = [\text{Ti}_{4.225}\text{Pb}_{1.51}\text{Sb}_{2.265}](\text{As}_{12.40}\text{Sb}_{7.60})\text{S}_{36}.$$

Comparison of the formulae indicates that the central part of the *T*₂ slab concentrates As with respect to the other slabs, with an As/(As + Sb)_{at} ratio of 0.62, to be compared with 0.51, 0.52 and 0.54 for *t*₁, *t*₂ and *T*₁ slabs.

The structural formula of chabournéite, as obtained during this crystal structure study, is $[\text{Ti}_{2.00}(\text{Pb}_{0.76}\text{Ti}_{0.11}\text{Sb}_{1.13})](\text{Sb}_{4.06}\text{As}_{4.94})\text{S}_{17}$, close to $[\text{Ti}_2(\text{Pb}_{0.8}\text{Ti}_{0.1}\text{Sb}_{1.1})](\text{Sb}_{4.1}\text{As}_{4.9})\text{S}_{17}$ (*Z* = 8).

4.2. Comparison with protochabournéite and dalnegroite

Orlandi *et al.* (2013) compared protochabournéite, chabournéite and dalnegroite. However, the lack of knowledge of the real structure of chabournéite precluded accurate comparisons. In the sub-cell structure Och of Pb-rich chabournéite (Nagl, 1979), the *t* and *T* slabs have the compositions $(\text{Ti}_4\text{Pb}_2\text{Sb}_2)_{\Sigma 8}(\text{Sb}_8\text{As}_8)_{\Sigma 16}\text{S}_{32}$ and $(\text{Ti}_4\text{Pb}_2\text{Sb}_2)_{\Sigma 8}(\text{Sb}_9\text{As}_{11})_{\Sigma 20}\text{S}_{36}$, respectively. These data compare well with the compositions of the *t*₁, *t*₂, *T*₁ and *T*₂ slabs obtained during the study of its refined structure. Consequently, the inner part of the *T* slabs preferentially concentrates As with respect to the inner part of the *t* slabs. This partitioning is the opposite of that observed in proto-

chabournéite, minor arsenic being preferentially concentrated in the inner part of the *t* slab.

Whereas in protochabournéite all (Sb,As) sites have Sb >> As, the arsenic and antimony distribution is more complex in chabournéite. In fact, in addition to pure Sb or As sites, 36 mixed (As,Sb) or (Sb,As) sites occur. Our study allows the comparison between the real As–Sb distribution obtained by us and those reported by Nagl (1979) for the sub-cell structure Och and Bindi *et al.* (2010) for dalnegroite. In both these structures, there is a strong partitioning between Sb and As that is not confirmed by the solution of the true structure Nch of chabournéite. Indeed, Nagl (1979) solved only the sub-cell and the cation distribution of Sb and As is actually more complicated, as pointed out by Orlandi *et al.* (2013) on the basis of bond-valence sums.

In dalnegroite, notwithstanding the solution of the true structure, there are some limitations due to the quality of the diffraction data and to the huge number of refined parameters (Bindi *et al.*, 2010). Nevertheless, there are some significant structural differences between dalnegroite and Pb-rich chabournéite:

(i) The unit-cell volume of dalnegroite is slightly over that of chabournéite, but its 16 Å parameter is below that of chabournéite (about 0.005% less). Such a volume increase is in contradiction with its higher (As/Sb)_{at} ratio, and is due to its higher Pb content.

(ii) When projected along the ~ 8.5 Å axis, with the same orientation of *t* ribbons, the in-plane angle of chabournéite is below 90° (*i.e.* 83.35°), whereas that of dalnegroite is over 90° (*i.e.* 96.38°). It indicates a ‘torsion’ of the crystal structure around the projection direction.

(iii) When projected along the ~ 16 Å axis (Fig. 6), a good atom layering parallel to (210) is observed for chabournéite and (012) for dalnegroite. This layering is quite perpendicular to *a* in chabournéite, giving a pseudo-orthorhombic symmetry [*b*' = 2*b* – *a*, *γ*' = 89.97 (20)°], missing in dalnegroite (*γ*' = 79°). In protochabournéite, *γ*' = 89.0 (1)°.

Thus, despite their close chemical compositions, dalnegroite and Pb-rich chabournéite show very distinct geometric characteristics, which does not favor a solid solution between these two species.

4.3. The chabournéite homeotypic series: further considerations

As defined by Orlandi *et al.* (2013), chabournéite, protochabournéite and dalnegroite are members of the chabournéite homeotypic series within the sartorite homologous series (Moëlo *et al.*, 2008). On the basis of the sub-cell of the members of this series, a general formula has been proposed, based on 13 cations and 17 S atoms: $[\text{Ti}_2 - x\text{Pb}_1 + 2x\text{Sb}_{1-x}]_{\Sigma=4}(\text{Sb}_{9-y}\text{As}_y)\text{S}_{17}$. The first part of the formula represents the mono-atomic zigzag surfaces hosting the heavy metals; the second part corresponds to the interlayer atoms belonging to the ‘thin’ and ‘thick’ slabs. The ideal structural formulae for protochabournéite and dalnegroite are well established, being

$[\text{Ti}_2\text{PbSb}](\text{Sb}_{7-8}\text{As}_{2-1})\text{S}_{17}$ and $[\text{Ti}_2\text{PbSb}](\text{Sb}_3\text{As}_6)\text{S}_{17}$, respectively (Orlandi *et al.*, 2013). On the contrary, the ideal structural formulae of chabournéite, as obtained from literature data, can be written as:

(i) $[\text{Ti}_2\text{PbSb}](\text{Sb}_5\text{As}_4)\text{S}_{17}$ (Jas Roux – Mantiene, 1974; Abuta – Johan *et al.*, 1981; Shimizu *et al.*, 1999);

(ii) $[\text{Ti}_2(\text{Ti}_{0.5}\text{Sb}_{0.5})\text{Sb}](\text{Sb}_4\text{As}_5)\text{S}_{17}$ (Jas Roux – Johan *et al.*, 1981);

(iii) $[\text{Ti}_2\text{PbSb}](\text{Sb}_4\text{As}_5)\text{S}_{17}$ (Jas Roux – Nagl, 1979; Abuta – Johan *et al.*, 1981; this study);

(iv) $[\text{Ti}_{1.5}\text{Pb}_2\text{Sb}_{0.5}](\text{Sb}_4\text{As}_5)\text{S}_{17}$, ideal composition close to the analysis of a ‘Pb-excess chabournéite derivative’ (Abuta – Johan *et al.*, 1981).

Consequently, two points should be discussed:

(i) Taking into account the first part of the formula, two well defined chemical poles exist, *i.e.* $[\text{Ti}_2\text{PbSb}]$ and $[\text{Ti}_2(\text{Ti}_{0.5}\text{Sb}_{0.5})\text{Sb}]$, corresponding to ‘Pb-rich’ and ‘Pb-free’ chabournéite, respectively. Although the crystal structure of Pb-free chabournéite has not been solved yet, these two poles are isotypic and microprobe analyses agree with a solid solution joining them. Whether Pb-rich chabournéite is a distinct mineral species relative to Pb-free chabournéite or not is subordinated to the crystallographical characterization of the ‘Pb-excess chabournéite derivative’ from Abuta. If this last compound is isotypic with the two other ones [and with Sb > As – see (ii)], Pb-rich chabournéite would simply correspond to a variety between the two other compounds.

(ii) Taking into account the second part of the formula, samples with compositions (Sb₅As₄) and (Sb₄As₅) exist, as well as (Sb₃As₆) for dalnegroite. This second point is a case of isovalent As³⁺ = Sb³⁺ substitution in the Pb-rich chabournéite, whose composition varies between $[\text{Ti}_2\text{PbSb}](\text{Sb}_5\text{As}_4)\text{S}_{17}$ and $[\text{Ti}_2\text{PbSb}](\text{Sb}_4\text{As}_5)\text{S}_{17}$. Even if in the second part of the formula (that represents the slabs’ composition) there are different (Sb/As)_{at} ratios, the known composition embraces the 50% mark $[\text{Ti}_2\text{PbSb}](\text{Sb}_{4.5}\text{As}_{4.5})\text{S}_{17}$ and considering the total sum (Sb + As), one has Sb ≥ As. On the other hand, dalnegroite, $[\text{Ti}_2\text{PbSb}](\text{Sb}_3\text{As}_6)\text{S}_{17}$, homeotypic with chabournéite, has Sb ≤ As.

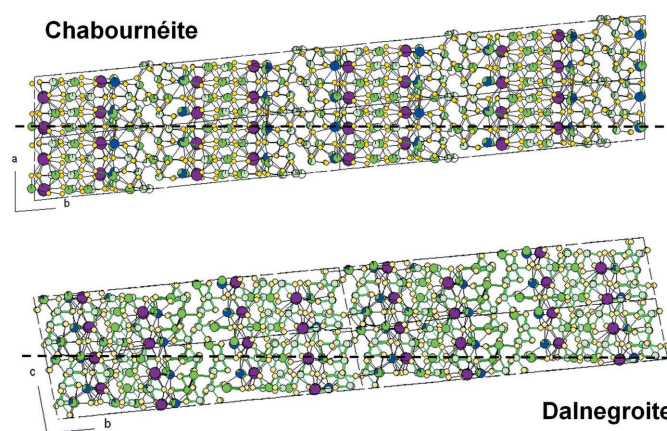


Figure 6
Atom layering in the crystal structures of chabournéite and dalnegroite.

5. Conclusion

The solution of the real crystal structure of Pb-rich chabournéite allows a better understanding of the crystal chemistry of this complex lead–antimony–arsenic sulfosalt and permits its comparison with its close homeotypes dalnegroite and protochabournéite. Nevertheless, a better understanding of the systematics of the chabournéite homeotypic series requires as priority the crystallographic characterization of ‘Pb-excess chabournéite derivative’ from Abuta, Japan. Secondary to this, it would be useful to solve the crystal structure of Pb-free chabournéite and to refine that of dalnegroite on the basis of a better single crystal.

Electron microprobe analyses were performed with the help of J. Langlade (engineer, ‘Microsonde Ouest’ laboratory, IFREMER, Plouzané, France). The authorities of the Parc National des Ecrins are warmly thanked for their support for the sampling and study of the Jas Roux mineralization. The valuable comments of Emil Makovicky and an anonymous reviewer helped us improve the paper.

References

- Berlepsch, P., Armbruster, T., Makovicky, E. & Topa, D. (2003). *Am. Mineral.* **88**, 450–461.
- Biagioni, C., Bonaccorsi, E., Moëlo, Y., Orlandi, P., Bindi, L., D’Orazio, M. & Vezzoni, S. (2014). *Mineral. Mag.* **79**, 101–117.
- Biagioni, C., D’Orazio, M., Vezzoni, S., Dini, A. & Orlandi, P. (2013). *Geology*, **41**, 747–750.
- Bindi, L., Nestola, F., Guastoni, A. & Secco, L. (2010). *Mineral. Mag.* **74**, 999–1012.
- Brese, N. E. & O’Keeffe, M. (1991). *Acta Cryst.* **B47**, 192–197.
- Bruker (2004). *APEXII*. Bruker AXS Inc., Madison, Wisconsin, USA.
- Campostrini, I., Demartin, F., Gramaccioli, C. M. & Russo, M. (2011). *Associazione Micro-mineralogica Italiana*, 344 p. Cremona, Italy.
- Cline, J. S., Hofstra, A. H., Muntean, J. L., Tosdal, R. M. & Hickey, K. A. (2005). *Econ. Geol.* 100th Anniversary Vol., 451–484.
- Engel, P. (1980). *Z. Kristallogr.* **151**, 203–216.
- Favreau, G., Bourgoin, V. & Boulliard, J. C. (2011). *Cah. Micromonteurs*, **113**, 92.
- Hofmann, B. A. & Knill, M. D. (1996). *Mineralium Deposita*, **31**, 319–339.
- Johan, Z. & Mantienné, J. (2000). *J. Czech. Geol. Soc.* **45**, 63–77.
- Johan, Z., Mantienné, J. & Picot, P. (1981). *Bull. Mineral.* **104**, 10–15.
- Makovicky, E. (1985). *Fortschr. Miner.* **63**, 45–89.
- Makovicky, E. (1993). *Eur. J. Mineral.* **5**, 545–591.
- Mantienné, J. (1974). Unpublished thesis, Université de Paris, 146 p.
- Moëlo, Y., Guillot-Deudon, C., Evain, M., Orlandi, P. & Biagioni, C. (2012). *Acta Cryst.* **B68**, 480–492.
- Moëlo, Y., Makovicky, E., Mozgova, N. N., Jambor, J. L., Cook, N., Pring, A., Paar, W., Nickel, E. H., Graeser, S., Karup-Møller, S., Balić Žunić, T., Mumme, W. G., Vurro, F., Topa, D., Bindi, L., Bente, K. & Shimizu, M. (2008). *Eur. J. Mineral.* **20**, 7–62.
- Nagl, A. (1979). *Z. Kristallogr.* **150**, 85–106.
- Nestola, F., Guastoni, A., Bindi, L. & Secco, L. (2009). *Mineral. Mag.* **73**, 1027–1032.
- Orlandi, P., Biagioni, C., Bonaccorsi, E., Moëlo, Y. & Paar, W. H. (2012). *Can. Mineral.* **50**, 235–251.
- Orlandi, P., Biagioni, C., Moëlo, Y., Bonaccorsi, E. & Paar, W. H. (2013). *Can. Mineral.* **51**, 475–494.
- Sheldrick, G. M. (1996). *SADABS*. University of Göttingen, Germany.
- Sheldrick, G. M. (2008). *Acta Cryst.* **A64**, 112–122.
- Shimizu, M., Matsuyama, F. & Shimizu, M. (1999). *Res. Geol.* **20**, 31–37.
- Volkov, A. V., Serafimovski, T., Kochneva, N. T., Tomson, I. N. & Tasev, G. (2006). *Geol. Ore Dep.* **48**, 175–192.
- Wedepohl, K. H. (1995). *Geochim. Cosmochim. Acta*, **59**, 1217–1239.
- Wilson, A. J. C. (1992). *International Tables for Crystallography*, Vol. C. Dordrecht: Kluwer Academic Publishers.
- Xiao, T. (2001). PhD Thesis, Université du Québec, 250 p.
- Zhou, T. F., Fan, Y., Yuan, F., Wu, M. A., Hou, M. J., Voicu, G., Hu, Q. H., Zhang, Q. M. & Yue, S. C. (2005). *Mineral. Petrol.* **85**, 243–251.